Normotopic Cortex Is the Major Contributor to Epilepsy in Experimental Double Cortex

Ludovic Franck Petit, PhD,[1,2] Marion Jalabert, PhD,[1,2]
Emmanuelle Buhler, MSc,[1,2,3] Arnaud Malvache, PhD,[1,2] Angélique Peret, MSc,[1,2]
Yoann Chauvin, MSc,[1,2] Françoise Watrin, PhD,[1,2]
Alfonso Represa, MD, PhD,[1,2] and Jean-Bernard Manent, PhD[1,2]

Objective: Subcortical band heterotopia (SBH) is a cortical malformation formed when neocortical neurons prematurely stop their migration in the white matter, forming a heterotopic band below the normotopic cortex, and is generally associated with intractable epilepsy. Although it is clear that the band heterotopia and the overlying cortex both contribute to creating an abnormal circuit prone to generate epileptic discharges, it is less understood which part of this circuitry is the most critical. Here, we sought to identify the origin of epileptiform activity in a targeted genetic model of SBH in rats.
Methods: Rats with SBH (*Dcx*-KD rats) were generated by knocking down the *Dcx* gene using shRNA vectors transfected into neocortical progenitors of rat embryos. Origin, spatial extent, and laminar profile of bicuculline-induced interictal-like activity on neocortical slices were analyzed by using extracellular recordings from 60-channel microelectrode arrays. Susceptibility to pentylenetetrazole-induced seizures was assessed by electrocorticography in head-restrained nonanesthetized rats.
Results: We show that the band heterotopia does not constitute a primary origin for interictal-like epileptiform activity in vitro and is dispensable for generating induced seizures in vivo. Furthermore, we report that most interictal-like discharges originating in the overlying cortex secondarily propagate to the band heterotopia. Importantly, we found that in vivo suppression of neuronal excitability in SBH does not alter the higher propensity of *Dcx*-KD rats to display seizures.
Interpretation: These results suggest a major role of the normotopic cortex over the band heterotopia in generating interictal epileptiform activity and seizures in brains with SBH.

ANN NEUROL 2014;76:428–442

Subcortical band heterotopia (SBH) or double cortex syndrome occurs when neocortical neurons fail to migrate to the correct location and accumulate in the white matter, forming a heterotopic band of neurons below the normally migrated or normotopic cortex.[1] This neuronal migration disorder is caused by mutations in the *DCX* gene and has an X-linked pattern of inheritance, with SBH in heterozygous female carriers, and lissencephaly in hemizygous males.[2–5] Rare SBH phenotypes in male patients with mosaic *DCX* mutations have also been reported.[3,6,7] Overall, mutations of *DCX* were identified in 100% of familial SBH phenotypes, and 85 to 90% of sporadic cases.[8,9]

SBH in humans is associated with mental retardation and epilepsy, with a high proportion of drug-resistant seizures.[8,10,11] Although both invasive (stereo electroencephalography [EEG]) and noninvasive (EEG combined with functional magnetic resonance imaging) electroclinical exploration of seizure generators were carried out in a few patients with SBH, it remains unclear

View this article online at wileyonlinelibrary.com. DOI: 10.1002/ana.24237

Received Feb 20, 2014, and in revised form Jul 8, 2014. Accepted for publication Jul 21, 2014.

Address correspondence to Dr Manent, INMED/INSERM U901, 163 Route de Luminy BP13, 13273 Marseille cedex 09, France.
E-mail: jean-bernard.manent@inserm.fr

From the [1]Institut de Neurobiologie de la Méditerranée/Institut National de la Santé et de la Recherche Médicale U901; [2]Aix-Marseille University; and [3]INMED/Plate-forme Post-Génomique de l'INMED, Marseille, France.

which structure in SBH or the normally migrated cortex is the most critical for generating abnormal activities. In these patients, epileptiform activities were recorded from both the heterotopic band and normotopic cortex, independently or not, and sometimes propagated to other brain structures.[12,13]

Experimental SBH can be modeled in rats by knocking down *Dcx* in embryonic brains using in utero RNA interference.[14–18] These *Dcx*-KD rats display altered neocortical excitability,[14] resulting in an increased propensity for convulsant-induced seizures at juvenile ages and spontaneous focal, absencelike seizures in adulthood.[16,17] Neurons located in SBH were found integrated within the same network as the overlying normotopic cortex, and both the heterotopic and normotopic cortices participated to epileptiform discharges.[14]

Therefore, although it is clear from animal and human studies that the band heterotopia and the overlying cortex both contribute to creating an abnormal circuit prone to generate epileptic discharges, it is less understood whether SBH is the origin of epileptiform activity. To investigate this issue, we performed 60-channel extracellular recordings from a microelectrode array (MEA) on neocortical slices from *Dcx*-KD rats, and electrocorticography in head-restrained nonanesthetized *Dcx*-KD rats. We show that the band heterotopia does not constitute a primary origin for interictal-like epileptiform activity in vitro and is dispensable for generating induced seizures in vivo. Furthermore, we report that most interictal-like discharges originating in the normotopic cortex secondarily propagate to the band heterotopia. Importantly, we found that in vivo suppression of neuronal excitability in SBH does not alter the higher propensity of *Dcx*-KD rats to display seizures, suggesting that the network reorganization previously reported in the normotopic cortex on its own may well contribute to seizure susceptibility.

Materials and Methods

Animal experiments were performed in agreement with European directive 2010/63/UE and received approval from the French Ministry for Research, after ethical evaluation by the institutional animal care and use committee of Aix-Marseille University (protocols #9-21032012 and #51-02112012).

In Utero Electroporation

We generated *Dcx*-KD animals and mismatch controls using in utero electroporation, as described before.[15,17] We used plasmid vectors encoding shRNAs targeting the 33′ untranslated region (3′UTR) of *Dcx* (3UTRhp, 1 μg/μl) or encoding ineffective shRNAs with 3 point mutations creating mismatches (3UTRm3hp, 1 μg/μl). Whereas the former construct efficiently knocks down *Dcx* expression in vivo, the latter construct is ineffective in causing *Dcx* knockdown.[15] Plasmid vectors were microinjected by pressure (PV 820 Pneumatic PicoPump; World Precision Instruments, Sarasota, FL) through the uterus of ketamine (IMALGENE 1000; Merial, Lyon, France; 100mg/kg)/xylazine (Rompun 2%; Bayer Healthcare, Leverkusen, Germany; 10mg/kg) anesthetized pregnant Wistar rats (Janvier, Le Genest-Saint-Isle, France) into the lateral ventricles of embryonic day 15 embryos by pulled glass capillaries (Drummond Scientific, Broomall, PA). Plasmids encoding green fluorescent protein (GFP) or monomeric red fluorescent protein (mRFP; CAG-GFP, 1 μg/μl; CAG-mRFP, 0.5 μg/μl) as reporter genes were electroporated concomitantly with vectors expressing shRNAs against *Dcx* or mismatch shRNAs. Electroporations were accomplished by discharging a capacitor with a sequencing power supply (BTX ECM 830 electroporator; BTX Harvard Apparatus, Holliston, MA). The voltage pulse (40V) was discharged across tweezer-type electrodes (Nepa Gene Co, Chiba, Japan) pinching the head of each embryo through the uterus.

For creating *Dcx*-KD rats with silenced SBH, RFP and Kir2.1 (CAG-Kir2.1, 1 μg/μl) expression plasmids were injected and electroporated together with plasmids encoding shRNAs against *Dcx* 3′UTR. For creating *Dcx*-KD rats with silenced SBH and normotopic cortex, a 2-step electroporation procedure was utilized: Kir2.1 and GFP expression plasmids were injected and electroporated 30 minutes before RFP and *Dcx* shRNA plasmids. As reported earlier, high coexpression levels of different transgenes can be obtained from multiple coelectroporated plasmids.[17,19] Here, we confirmed that only $3.15 \pm 0.8\%$ of RFP-expressing neurons coelectroporated with *Dcx* shRNAs plasmids were Dcx-immunopositive, whereas $77.8 \pm 2.0\%$ of RFP-expressing neurons coelectroporated with mismatch shRNAs were Dcx-immunopositive on primary cortical neuron cultures (363 and 219 neurons were analyzed; *t* test; $p < 0.0001$). Furthermore, we confirmed that ~90% of GFP-expressing neurons coelectroporated with Kir2.1 plasmids functionally expressed Kir2.1 channels on cultivated slices (16 of 18 neurons) and 100% of them on acute neocortical slices (5 of 5 neurons). Together, these data suggest that a large proportion of fluorescent, transfected neurons also coexpress either effective *Dcx* shRNAs and/or functional Kir2.1 channels.

Intracortical EEG Recordings

Recordings were performed from head-restrained nonanesthetized rats from postnatal day (P) 13 to P17 ($n = 47$) as described previously.[20] Stereotaxic surgeries for electrophysiology were performed under isoflurane anesthesia. Rat pups were anesthetized initially with 3% isoflurane in air that was administered through a facemask. Buprenorphine (buprecare; Axience, Mumbai, India; 0.03mg/kg, 0.03mg/ml) was injected subcutaneously before the surgery and a local anesthetic (lidocaine [Xylovet]; Ceva Sante Animale, Libourne, France) was infiltrated under the skin at all incision points. During surgery, the concentration of isoflurane was kept at 1.0 to 1.5%. The skull was exposed and covered by dental acrylic except a bone part above the somatosensory cortex to allow electrode implantation. Following a recovery period, animals were placed in a

stereotaxic frame, and body temperature was maintained at 37°C, using a heating pad. The animal head was restrained using dental acrylic fixation between the nose bar and frontal bone and between ear bars and occipital bone not to hurt animals during the restraining. Under isoflurane anesthesia (1.0–1.5%), holes were drilled to lower reference electrodes within the cerebellum and recording electrodes within the somatosensory cortices of the 2 hemispheres. Recording electrodes (paraformaldehyde-insulated, single-stranded stainless steel wires; bare diameter = 0.003in; A-M Systems, Carlsborg, WA) in the somatosensory cortices were inserted at the following coordinates: −1mm from bregma, 5mm from midline, and 1.5mm from brain surface. Through these electrodes and after a recovery period of 30 minutes, extracellular field potentials were recorded versus references, amplified 1,000× using a custom-built amplifier, and digitized at 10kHz through a Digidata 1440 interface (Axon Instruments, Sunnyvale, CA). After a 30-minute baseline, pentylenetetrazol (PTZ) was administrated (Sigma-Aldrich, St Louis, MO; 25mg/kg, intraperitoneally) every 10 minutes until seizure occurrence. Valium (Roche, Basel, Switzerland; 2.5mg/kg, intraperitoneally) was injected to stop seizures lasting >5 minutes. The number of PTZ injections triggering seizures and seizure latency were analyzed.

Histological Analysis

At the end of each in vivo experiment, rats were deeply anesthetized with pentobarbital and perfused. Brains were removed, sectioned (100 μm coronal sections) with a vibrating microtome (Microm HM 650V; Thermo Scientific, Waltham, MA), and mounted on glass slides. Both for determination of recording electrode site after intracortical EEG recordings and for SBH characterization, microphotographs were taken using an Olympus (Tokyo, Japan) SZX16 fluorescent stereomicroscope. Rostrocaudal extent, size, and position of SBH were measured. The last 2 parameters were quantified at the level of the bregma reference. SBH position was determined by calculating distances between the SBH center of mass and an anatomical reference below the somatosensory cortex. To define the anatomical reference, a horizontal line starting below the corpus callosum was drawn perpendicularly to the section midline. This horizontal line intersects with the gray–white matter border below the somatosensory cortex at a unique location. Neocortical sections were manually reconstructed in Photoshop (Adobe Systems, San Jose, CA). For coexpression analysis, microphotographs were taken using a Leica (Wetzlar, Germany) TCS SP5 X confocal microscope using ×20 objectives. Neurons coexpressing RFP and GFP were counted in Fiji/ImageJ 1.45b,[21] using a cell-counter plugin (Kurt De Vos, University of Sheffield, Sheffield, United Kingdom). Abbreviations and structure limits are based on the postnatal rat brain in stereotaxic coordinates at P14 (Zaynutdinova-Khazipov et al, unpublished data).

Multisite Recordings from Microelectrode Arrays

Brains from P15 *Dcx*-KD and mismatch pups were rapidly removed and placed in oxygenated ice-cooled artificial cerebrospinal fluid (ACSF) with the following composition (in millimolars): 126 NaCl, 3.5 KCl, 2 $CaCl_2$, 1.3 $MgCl_2$, 25 $NaHCO_3$, 1.2 $NaHPO_4$, and 10 d-glucose (95% O_2 and 5% CO_2, pH 7.4). Coronal neocortical slices (400 μm) were obtained with a vibrating microtome (Microm International, Walldorf, Germany) and kept in oxygenated ACSF at room temperature at least 1 hour before use. Substrate-integrated MEAs (Multi Channel Systems, Reutlingen, Germany) were used to record neuronal activity, as described with modifications.[22] MEAs comprised 59 electrodes of 50 μm diameter in a 6 × 10 arrangement with 500 μm spacing between electrodes or 60 electrodes of 30 μm diameter, in an 8 × 8 arrangement with 200 μm spacing between electrodes. Individual slices were then transferred to the recording chamber, where they were fully submerged and superfused with 30°C ACSF at a rate of 2ml/min. Slice position upon the MEA was determined by observation with an Olympus SZX16 stereomicroscope. Once positioned, slices were immobilized using a grid. Epileptiform activity was induced by bath application of the γ-aminobutyric acid $(GABA)_A$ receptor antagonist bicuculline methochloride (Tocris, Bristol, United Kingdom). Slices were first recorded in the absence of any drug for 20 minutes to monitor spontaneous activity. Then, bicuculline was bath applied at increasing concentrations (0.5 μM, 1 μM, and 2 μM) every 20 minutes, and epileptiform activity was recorded for 20 minutes at the highest concentration (2 μM). Recordings were performed using MC Rack software (Multi Channel Systems), and electrode raw data were digitized at 10kHz after amplification (1,100 × gain). At the end of the recordings, slices were photographed under fluorescent light and bright field with a CCD camera (Motic, Hong Kong).

Analysis of MEA Signals

Detection of interictal-like events (ILEs) was performed on 3 to 200Hz bandpass filter after downsampling the electrode raw data to 1kHz, using a custom-written program in Matlab (MathWorks, Natick, MA). A 2-step detection procedure was utilized: first, events with amplitudes >5× the standard deviation (SD) of the signal for the whole recording period were roughly detected for each MEA channel. Next, onsets of individual events for each MEA channel were more precisely determined using a threshold based on the calculated SD from the signal of the second preceding the detected event. For individual ILEs, the MEA channel with the earliest onset was detected and the recruitment onset for other subsequently active MEA channels was calculated. Based on the calculated MEA channel recruitment delays and the shape of the local field potential (LFP), an experimenter blind to the condition analyzed was then prompted by the program to determine the MEA channel from which the LFP with the sharpest negativity peak and the highest amplitude was first recorded. Events with confirmed origins of onset were further analyzed, and inadequately detected events or artifacts were discarded.

Hierarchical clustering was utilized to classify detected events. We developed a custom clustering algorithm in Matlab that determined the groupings based on statistical significance

(see Feldt Muldoon et al[23]). This algorithm grouped events with statistically similar spatiotemporal dynamics. It did not require a priori knowledge of the number of groups. The algorithm relied on a 2-step method that classifies events first regarding their temporal dynamics (ie, MEA channel recruitment onsets) and second with respect to their spatial shape (ie, maps of involved MEA channels). The classifications were based on pairwise similarity metrics adapted to our specific measurements. The statistically closest events with respect to these metrics were then grouped together using an agglomerative hierarchical cluster tree based on the shortest distance between statistical significances (linkage method using average distance). The clusters were finally defined by cutting the tree at a threshold of 0.05. To rigorously compare the origins of onset of interictal-like activity between rats and experimental conditions, we used a custom-written program in Matlab that unfolds the neocortex and converts it into standardized rectangles. First, the outer and inner contours of the cortex were manually selected, as well as 2 opposite corners of the MEA grid and the SBH contour. The cortex contours were interpolated using a fourth-order polynomial fit. We then defined a new set of coordinates (L, H) where L was the linear coordinate along the inner cortex (arc length) and H the distance from the inner cortex; H was normalized for each position L so that $H = 0$ on the inner cortex and $H = 1$ on the outer cortex. Finally, the manually selected Cartesian coordinates of the SBH contour and the MEA grid were converted to the standardized coordinates (L, H) using the explicit equations of the cortex contours.

Current source density analysis was performed from ILEs recorded from a linear array of 7 MEA channels (interelectrode distance = 200 μm) covering a cortical column above SBH in *Dcx*-KD rats or at a similar location in mismatch. For each recording, amplitudes of 5 randomly chosen ILEs were normalized, temporally aligned with respect to the onset of the LFP events having the sharpest negative peak and highest amplitude, and averaged. Current source density was calculated for the averaged ILE according to Nicholson and Freeman[24] in Matlab, and a 3-dimensional map with color-coded current source density (CSD) values was drawn.

Multiunit activity (MUA) detection was performed with MC-Rack software. A high-pass filter (Butterworth second order) was applied at 300Hz on raw signals. Spikes with amplitude > 3 SD were automatically detected within MC-Rack. The proportion of LFP events associated with MUA was quantified, as well as the mean number of detected spikes per population event.

Patch Clamp Recordings on Cultivated and Acute Slices

Hippocampal slices (400 μm) from P5 wild-type rats were prepared using a McIlwain tissue chopper (The Mickle Laboratory Engineering Co. Ltd., Guildford, Surrey, UK) and transferred to the electroporation chamber (Nepa Gene Co, Chiba, Japan) containing cold phosphate-buffered saline/glucose (0.6%). Plasmids encoding GFP (CAG-GFP, 1 μg/μl) and Kir2.1 (CAG-Kir2.1, 1 μg/μl), or GFP alone were microinjected by pressure (Picospritzer; General Valve Corporation, Fairfield, NJ) into the brain tissue using a glass capillary (Drummond Scientific). Voltage pulse (25V) was given through a round-shaped electrode that was positioned onto the slice surface using a micromanipulator. Electroporated slices were then cultivated at 37°C with 5% CO_2 and 95% air onto the membrane of Millicell-CM inserts (Millipore, Billerica, MA) in a minimum essential medium supplemented with horse serum (20%) and insulin (25 μg/ml). After 2 or 3 days in vitro, cultured slices were placed in a recording chamber, where they were fully submerged and superfused at a 2 to 3ml/min flow rate with an oxygenated ACSF (see above). Acute neocortical slices from P15 rat brains were prepared as described above. GFP-expressing neurons were visualized with a fluorescent upright microscope equipped with an appropriate filter and recorded using the patch clamp technique in the whole cell configuration. Microelectrodes had a resistance of 5 to 10MΩ and were filled with a solution containing the following (in millimolars): 130 $KMeSO_4$, 5 KCl, 5 NaCl, 10 HEPES-K, 2.5 MgATP, 0.3 NaGTP, pH = 7.25. Whole cell measurements in current clamp mode were digitized using Axoscope (Molecular Devices, Sunnyvale, CA) and Pulse (HEKA Elektronik, Lambrecht/Pfalz, Germany). Data were analyzed using Clampfit (Molecular Devices) and MiniaAnalysis (Synaptosoft, Decatur, GA).

Statistical Analysis

Statistical analysis was performed using Prism 6.01 (GraphPad Software, La Jolla, CA). Normality of data distribution was checked with the d'Agostino and Pearson omnibus test, and parametric or nonparametric tests (listed in the main text) were used accordingly. All data are presented as mean ± standard error of the mean.

Results

Dcx-KD Rats Display Subcortical Band Heterotopia and Increased Susceptibility to PTZ-Induced Seizures

We created rats with SBH using in utero electroporation and RNAi-mediated *Dcx* knockdown. Plasmids encoding shRNAs against the 3′UTR of *Dcx* were injected into the cerebral ventricles of embryonic day 15 rat embryos and were electroporated into a subset of neural progenitors to initiate SBH formation and laminar displacement, as described.[14–18] Our control animals (mismatch) were created by utilizing shRNAs with 3 point mutations creating mismatches, making them ineffective at causing *Dcx* knockdown. Both control and *Dcx*-KD rats expressed either red or green fluorescent proteins in the targeted neuronal population for facilitating its visualization.

To characterize histopathological features of our rat model, we first measured the rostrocaudal extent, size, and position of SBH at P15 in a group of 6 *Dcx*-KD rats. In 6 of 6 *Dcx*-KD rats, we consistently observed bandlike structures resembling SBH at the gray–white

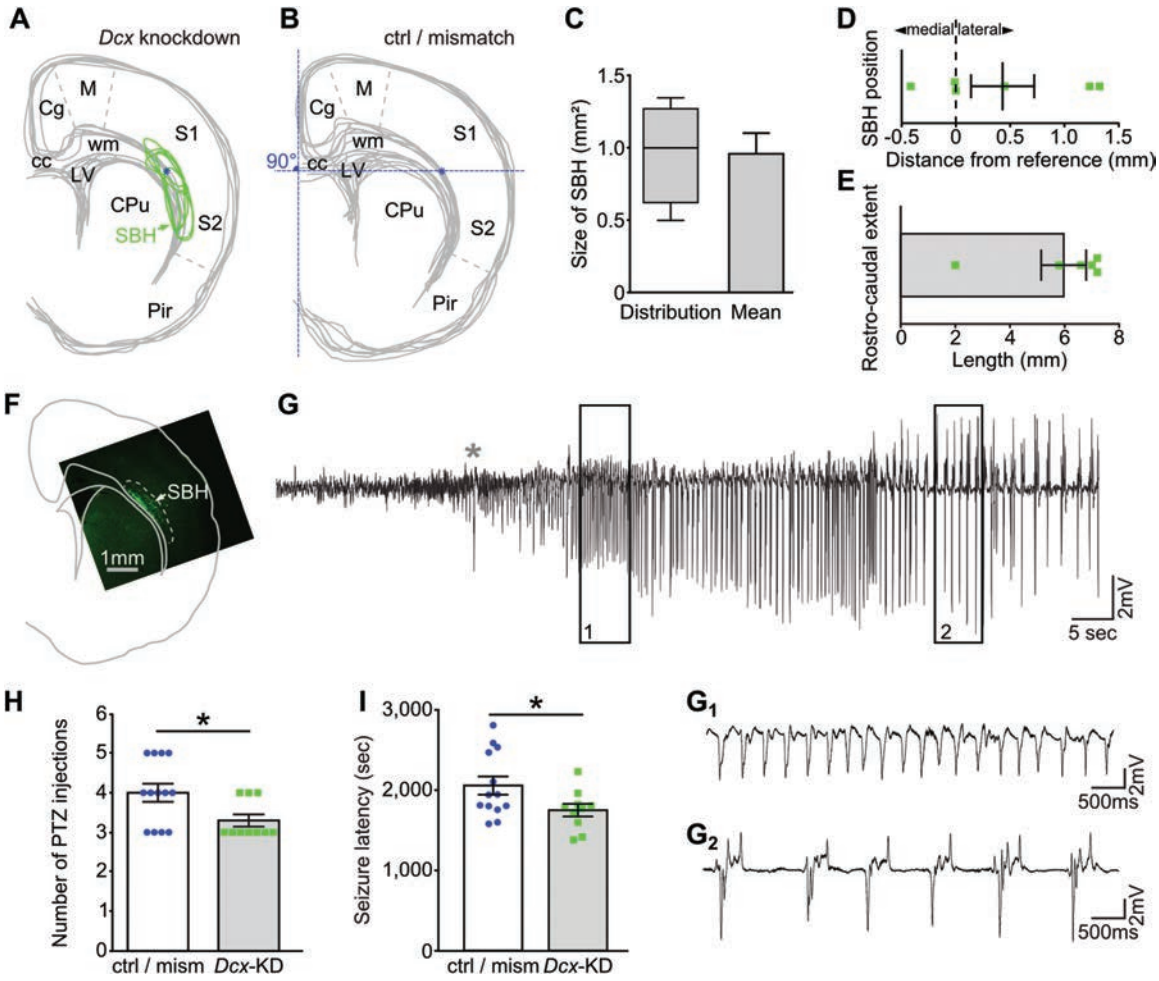

FIGURE 1: *Dcx*-KD rats display subcortical band heterotopia below the somatosensory cortex and exhibit increased susceptibility to pentylenetetrazol (PTZ)-induced seizures. (A, B) Reconstructed neocortical sections positioned at bregma from 6 *Dcx*-KD rats (A) and 7 mismatch controls (B). Green lines delineate subcortical band heterotopias (SBHs), and asterisk shows the anatomical reference. cc = corpus callosum; Cg = cingulate cortex; CPu = caudate putamen; LV = lateral ventricle; M = motor cortex; Pir = piriform cortex; S1 = primary somatosensory cortex; S2 = secondary somatosensory cortex; wm = white matter. (C) Box plot and bar graph showing size distribution and mean size of SBH. In the box plot, the horizontal line shows the median, and whiskers show minimum/maximum values. In the bar graph, mean values ± standard error of the mean (SEM) are given. (D) Scatter dot plot showing the position of SBH center of mass relative to the anatomical reference (*vertical dashed line* on the plot = *asterisk* in B). Vertical bar and error bars show mean and SEM, respectively. (E) Bar graph and scatter dot plot showing the rostrocaudal extent of SBH. Mean values ± SEM are given. (F) Microphotograph of a neocortical section from a *Dcx*-KD rat showing the recording site and SBH. (G) Representative intracortical electroencephalographic (EEG) recording from a *Dcx*-KD rat showing a PTZ-induced electrographic seizure. Seizure initiation is characterized by a single EEG spike *(asterisk)*, followed by high-amplitude, high-frequency spiking activity, which progresses into a regular spiking activity at the tonic phase of the seizure (box 1, shown enlarged in G_1). The clonic phase of the seizure comprises large-amplitude waves containing multiple EEG spikes (box 2, shown enlarged in G_2), and is associated with a reduction in frequency. (H, I) Bar graph and scatter dot plot illustrating the mean number of PTZ injections leading to electrographic seizures (H) and the mean latency to PTZ-induced seizures (I) in control/mismatch (ctrl/mism) and *Dcx*-KD rats (13 and 10 rats, respectively). Mean values ± SEM are given. *$p < 0.05$.

matter border below the somatosensory cortex, and extending within both deep cortical layers and white matter (Fig 1A). Rostrocaudally, these SBH extended over a mean length of 5.9 ± 0.8mm from their most rostral end located on average 1.8 ± 0.8mm rostral to bregma. At bregma, the size of SBH averaged 0.9 ± 0.1mm^2, and SBH centers of mass were located 0.4 ± 0.3mm from an anatomical reference (see Materials and Methods) below the somatosensory cortex (see Fig 1C–E). Control rats generated using the same experimental procedure but with ineffective shRNAs never displayed any detectable histopathological abnormalities (see Fig 1B).

To assess for the presence of EEG abnormalities, we next performed intracortical EEG recordings in 10 head-restrained nonanesthetized *Dcx*-KD rats and 13 controls. We bilaterally implanted 2 recording electrodes at stereotaxic coordinates corresponding to the most

rostral third of the brain portion containing SBH, as extrapolated from the histopathological data described above. In all implanted rats, post hoc histological analyses confirmed both the presence of SBH (see Fig 1F) and the appropriate positioning of electrode implantation sites. Thirty-minute baseline recordings of the ongoing activity in head-restrained P13–17 *Dcx*-KD rats did not reveal any spontaneous epileptiform events, in keeping with what we previously observed in freely moving P12 to P15 *Dcx*-KD rats.[16] Control rats never displayed EEG abnormalities either. To evaluate whether the presence of SBH in *Dcx*-KD rats is associated with an increased susceptibility to induced seizure, we intraperitoneally administered *Dcx*-KD rats and controls with a series of subconvulsive doses of PTZ (25mg/kg) every 10 minutes while recording their intracortical EEG. As compared to control rats, we recorded electrographic seizures in *Dcx*-KD rats at significantly lower doses of PTZ (82.50 ± 3.82mg/kg in *Dcx*-KD rats and 100 ± 5.66mg/kg in control/mismatch; unpaired t test, $p < 0.05$) and with significantly shorter latencies ($1{,}755 \pm 78.99$ seconds in *Dcx*-KD rats and $2{,}063 \pm 113.30$ seconds in control/mismatch; unpaired t test, $p < 0.05$; see Fig 1G–I). Once evoked, seizures in control and *Dcx*-KD rats were similar, for all parameters we analyzed (not shown), and always comprised a tonic and a clonic phase (see Fig 1G).

Thus, *Dcx*-KD rats consistently display SBH resembling those seen in patients, and the presence of such malformation contributes to creating an altered neocortical circuitry associated in rats with an increased propensity for convulsant-induced seizures.

Interictal-like Activity in Neocortical Slices Can Be Decomposed into Groups of Interictal-like Events Sharing Highly Similar Spatiotemporal Dynamics

To investigate which part of the altered neocortical circuitry—SBH or the overlying cortex—might underlie the increased propensity for induced seizures in *Dcx*-KD rats, we prepared neocortical slices from P15 rats with SBH and controls and made extracellular recordings using 60-channel MEAs. In keeping with our intracortical EEG recordings and previous report,[14] 20-minute extracellular recordings in normal ACSF did not reveal any spontaneous epileptiform activity in slices from *Dcx*-KD rats. We then tested whether slices from *Dcx*-KD rats were capable of generating epileptiform activity when perfused with 2 μM bicuculline, an antagonist of $GABA_A$ receptors. As expected, interictal-like epileptiform activity composed of synchronous epileptiform ILEs was generated under this condition in all slices from *Dcx*-KD rats (Fig 2A) and controls, and LFPs were simultaneously recorded from multiple MEA channels (see Fig 2A, B). Amplitude, duration of ILEs, and interevent interval as measured from a selected MEA channel were not significantly different in slices from *Dcx*-KD rats and controls (not shown), suggesting that slices with SBH have a similar threshold for generating epileptiform activity as control slices with no SBH, although *Dcx*-KD rats have lower thresholds than controls for induced seizures in vivo.

To further characterize interictal-like activity in slices from *Dcx*-KD and control rats, we identified for each ILE the MEA channel from which the LFP with the sharpest negativity peak and highest amplitude was first recorded and then measured the recruitment onset for other subsequently active MEA channels. Color-coded pixel maps showing the recruitment delays for each MEA channel were constructed to represent the spatiotemporal dynamics of MEA channel recruitment onset for individual ILEs (Fig 2). To further search for statistically significant similarities between spatiotemporal dynamics of MEA channel recruitment onsets for individual ILEs, we designed a clustering algorithm based on chosen similarity metrics (see Materials and Methods and Feldt Muldoon et al[23]). In brief, this algorithm sequentially groups ILEs based on the temporal dynamics of MEA channel recruitment onsets and on the spatial distance between recruited MEA channels, and a dendrogram representing the order of grouping is generated. A statistical significance cutoff determining the point at which the grouping is no longer statistically significant is calculated, and a common color is attributed to ILEs that have been grouped below this threshold in the dendrogram. This analysis revealed that interictal-like activity in neocortical slices from both *Dcx*-KD and control rats can be decomposed in a limited number of clusters that was not significantly different in the 2 conditions (2.8 ± 0.2 clusters/slice in mismatch rats; 2.5 ± 0.2 clusters/slice in *Dcx*-KD rats; unpaired t test, $p = 0.3$). On average, the major cluster was found to comprise >60% of the ILEs recorded from a given slice ($63.8 \pm 7.4\%$ in mismatch and $64.4 \pm 6.1\%$ in *Dcx*-KD), the distribution of ILEs between clusters being not significantly different in slices from *Dcx*-KD or control rats, nor the total number of recorded ILEs.

Taken together, these observations suggest that neocortical slices are capable of generating highly stereotyped interictal-like activity composed of groups of ILEs sharing similar spatiotemporal dynamics, thus enabling a reliable characterization of both the origin and spatial extent of interictal-like activity in slices with SBH, as compared to control slices.

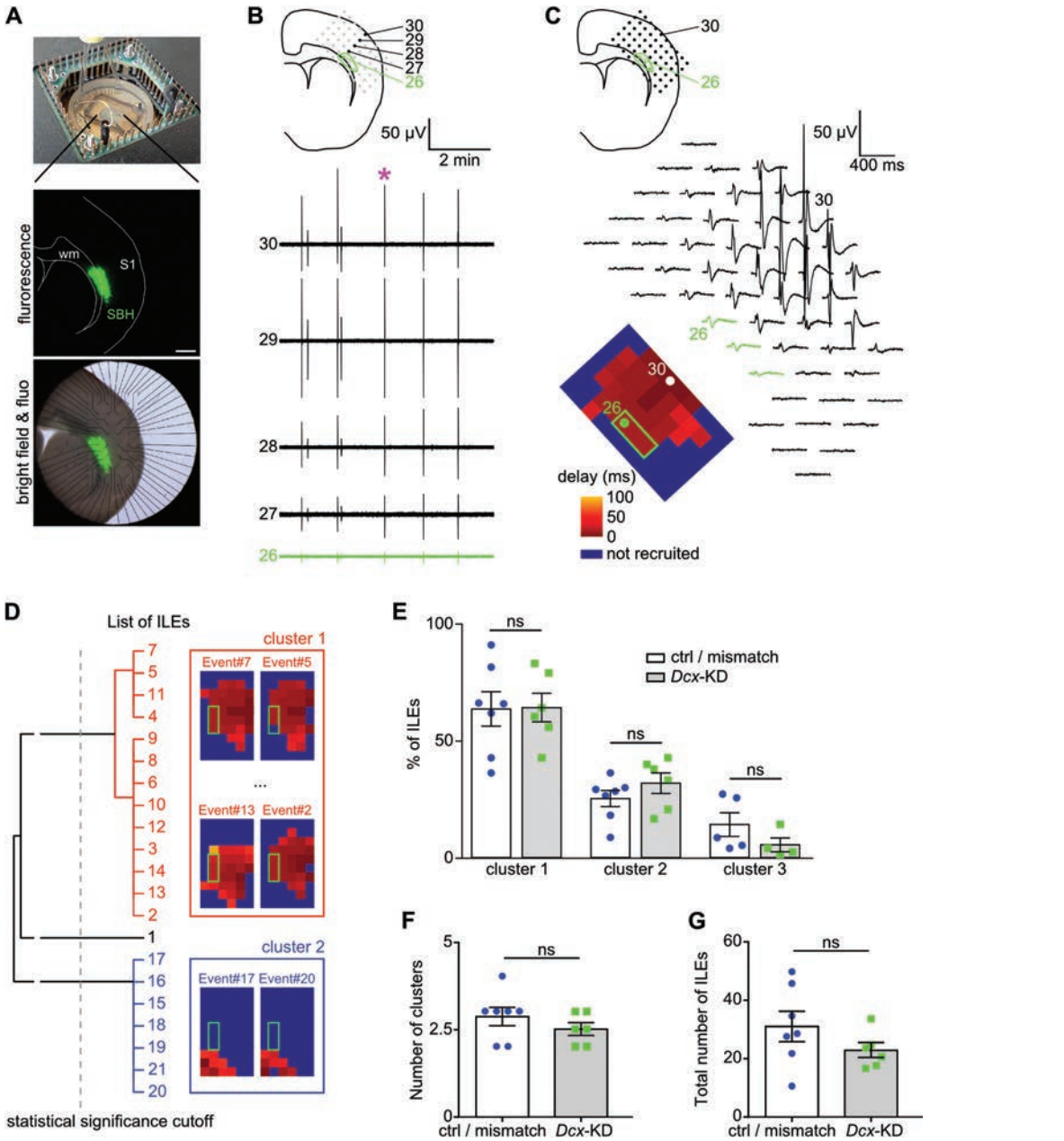

FIGURE 2: Interictal-like activity in neocortical slices can be decomposed into groups of interictal-like events (ILEs) sharing highly similar spatiotemporal dynamics. (A) Top panel: photograph showing the microelectrode array (MEA) recording chamber containing a neocortical slice. Bottom panels: fluorescent and composite microphotographs of a neocortical section from a *Dcx*-KD rat, as mounted on the MEA grid. Green fluorescent protein–expressing fluorescent neurons forming SBH are in green. S1 = primary somatosensory cortex; SBH = subcortical band heterotopia; wm, white matter. (B) Top panel: a schematic view showing the spatial arrangement of the MEA grid on a neocortical slice from a *Dcx*-KD rat. Green lines delineate SBH boundaries. Bottom panel: interictal-like activity in a *Dcx*-KD rat, as simultaneously recorded from 5 selected MEA channels (out of 60 MEA channels) located in the normotopic cortex (*black traces,* channels 27–30) and in SBH (*green trace,* channel 26). Asterisk marks the ILE shown at higher timescale in C. (C) An ILE, as simultaneously recorded from 60 MEA channels. Traces are arranged according to the topology of MEA channels on the slice (shown in the top panel). Signals recorded from the 3 SBH-located MEA channels are showed in green. The color-coded pixel map illustrates the spatiotemporal dynamics of MEA channels recruitment onset for the same event. Green rectangle delineates MEA channels located in SBH. (D) Left, dendrogram representing hierarchically clustered ILEs recorded from a *Dcx*-KD rat, and obtained using a clustering algorithm based on the temporal dynamics and spatial shape of events. The statistically closest ILEs with respect to their spatiotemporal dynamics are grouped together using an agglomerative hierarchical cluster tree based on shortest distances between probability values. Right: representative pixel maps of selected ILEs belonging to the different clusters. (E) Bar graph and scatter dot plots showing the percentage of ILEs distributed in each cluster in control (ctrl)/mismatch and *Dcx*-KD rats. Note that the major cluster comprises >60% of events. ns = not significant. (F) Bar graph and scatter dot plots illustrating the mean number of clusters obtained after analyzing interictal-like activity in control/mismatch and *Dcx*-KD rats. (G) Bar graph and scatter dot plots showing the total number of ILEs recorded and analyzed in control/mismatch and *Dcx*-KD rats. Interictal-like activity from n = 7 control/mismatch rats and n = 6 *Dcx*-KD rats was analyzed. Mean values ± standard error of the mean are given.

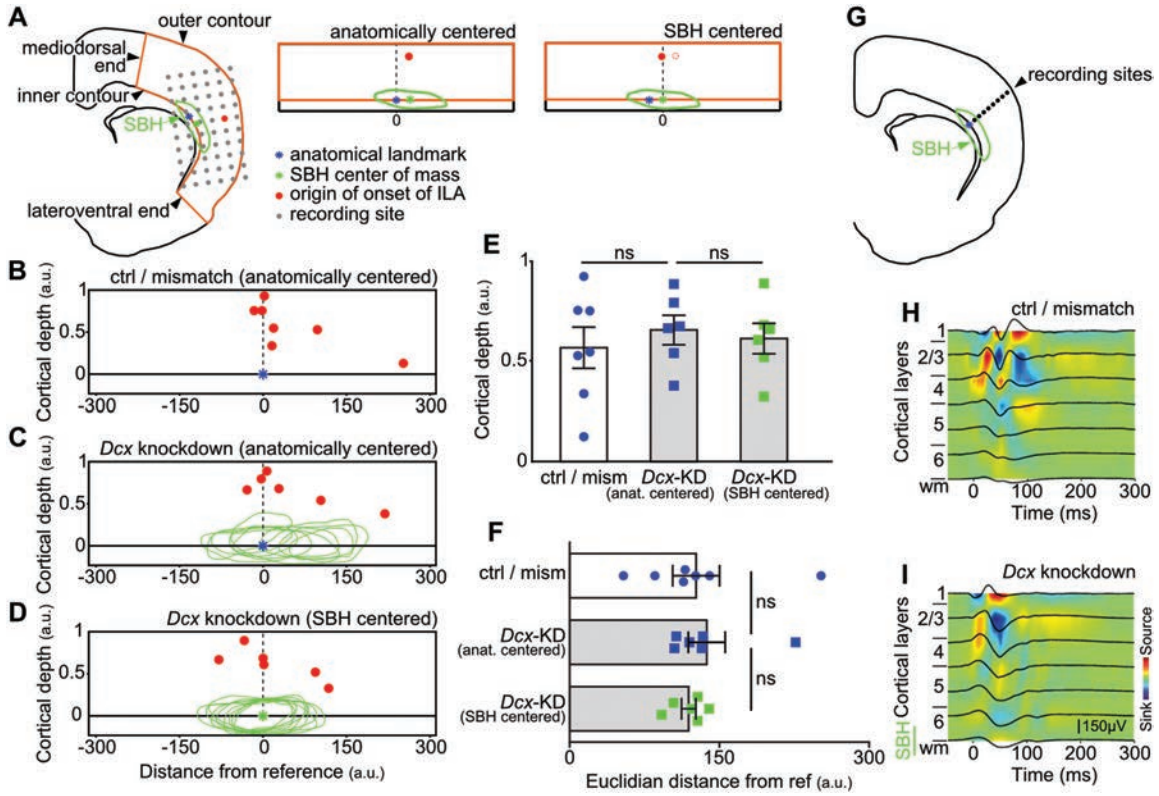

FIGURE 3: Interictal-like activity (ILA) in neocortical slices does not originate in subcortical band heterotopia (SBH), but within the most superficial layers of the overlying cortex. (A) Recorded neocortical areas are standardized using a normalization procedure that unfolds the neocortex and converts it in standardized rectangles. Spatial origins of onset of interictal-like activity are plotted either relative to an anatomical reference (ie, anatomically centered) or with respect to the SBH center of mass (ie, SBH centered). SBH boundaries are delineated in green. (B–D) Origins of onset of ILA as a function of the cortical depth in standardized somatosensory cortices of wild-type/mismatch rats (B) and *Dcx*-KD rats (C, D) aligned with respect to the anatomical landmark (C) and to the SBH center of mass (D). a.u. = arbitrary units; ctrl = control. (E, F) Bar graphs and scatter dot plots showing the cortical depth of the origins of onset (E), and its Euclidian distance from the anatomical (anat.) reference (ref; F) in control (ctrl)/mismatch (mism) and *Dcx*-KD rats. ns = not significant. (G–I) Normalized and averaged local field potential traces as recorded from 7 MEA channels on a cortical column (G) in the somatosensory cortex of a control/mismatch (H) and a *Dcx*-KD (I) rat superimposed with color-coded maps showing current source density analysis. ILA from n = 7 control/mismatch rats and n = 6 *Dcx*-KD rats was analyzed. Mean values ± standard error of the mean are given. wm = white matter.

Interictal-like Activity in Neocortical Slices Does Not Originate in SBH, but within the Most Superficial Layers of the Overlying Cortex

We characterized the spatial origin of interictal-like activity in *Dcx*-KD and control rats by focusing our analysis on ILEs belonging to the major cluster, as determined by the clustering algorithm described above. To make an accurate statistical evaluation of data obtained from different slices and experimental conditions, we first applied a normalization procedure that unfolds the somatosensory cortex and converts it in standardized rectangles (Fig 3). This allowed us to plot all individual origins of interictal-like activity on a 2-dimensional map illustrating their laminar position, with all data sets aligned with respect to the anatomical references (ie, anatomically centered) or to the SBH centers of mass (ie, SBH centered). When analyzing the laminar position of individual origins in anatomically centered slices from *Dcx*-KD rats, we found that no origins were located within SBH boundaries; they were instead located within the overlying normotopic cortex, suggesting that interictal-like activity originates in the latter structure and not in SBH. Anatomically, in both *Dcx*-KD and mismatch rats, these origins in the somatosensory cortex were mostly found aligned above the anatomical reference (in 5 of 7 mismatch rats and in 4 of 6 *Dcx*-KD rats), and a few were located more laterally and ventrally. On average, the origins of onset of interictal-like activity were located at a similar depth in the cortex, roughly corresponding to intermediate and superficial cortical layers, in both *Dcx*-KD and mismatch rats. To further assess for a difference in the lateral dispersion of individual origins in *Dcx*-KD and mismatch rats, we compared in these 2 groups the Euclidian distance of individual origins relative to the anatomical reference and found no significant difference in the mean distance.

To investigate whether SBH position exerted an influence over the laminar position of individual origins of interictal-like activity, we aligned all data sets with respect to SBH centers of mass. In SBH centered slices from *Dcx*-KD rats, we observed that individual origins were uniformly distributed in the overlying normotopic cortex, all being located in a portion of somatosensory cortex directly facing SBH, and not extending beyond these limits (see Fig 3D). Because neither the mean cortical depths of the origins of onset nor their mean Euclidian distances were significantly different in both anatomically centered and SBH centered slices from *Dcx*-KD rats (see Fig 3E, F), this suggests that no specific portion of the somatosensory cortex seems to constitute a preferential origin for interictal-like activity in *Dcx*-KD rats. However, the portion of neocortex directly facing SBH, and not those located more dorsally and medially to SBH or more laterally and ventrally, appears more prone to generate interictal-like activity (see Fig 3D).

Because our analysis was based on raw LFPs, we further confirmed our observations by examining the contributions of different cortical layers to the initiation of interictal-like activity using CSD analysis. CSD analysis provided us with a more accurate estimation of the laminar location of transmembrane currents underlying ILEs. We took advantage of the finding that most origins were aligned above the anatomical reference in both mismatch and *Dcx*-KD rats, and made extracellular recordings from 7 MEA channels (interelectrode distance = 200 μm) covering an entire cortical column above this reference (see Fig 3G). In both mismatch and *Dcx*-KD rats, CSD analysis of normalized and averaged ILEs revealed in cortical layers 2–3 a large current sink that coincides with the sharpest negative peak of the LFP (see Fig 3H, I). Overall, the most intense current flows were observed in upper cortical layers, suggesting that the neuronal populations generating interictal-like activity are located in these layers, in keeping with the above observations and our previous report.[14]

Last, we confirmed that the majority of LFP events recorded at the origin of onset were associated with multiunit firing in both *Dcx*-KD and mismatch rats ($89.33 \pm 6.3\%$ and $91.23 \pm 7.3\%$ of ILEs, respectively; see below and Fig 4E). On average, the number of detected spikes per LFP event was not different in the 2 conditions (8.08 ± 2.53 in *Dcx*-KD rats and 9.29 ± 2.41 in mismatch; unpaired *t* test, not significant).

Altogether, these observations suggest that interictal-like epileptiform activity in *Dcx*-KD rats does not originate in SBH but within the most superficial layers of the overlying cortex.

Interictal-like Activity Originating in the Overlying Cortex Secondarily Propagates to SBH

After we identified the spatial origin of interictal-like activity in *Dcx*-KD rats and controls, we next investigated its spatial extent and propagation over neocortical slices. Similarly to what was done in the above section, we focused our analysis on ILEs belonging to the major cluster. We defined the spatial extent of an individual ILE as the percentage of MEA channels that recorded extracellular signals during this event. Consequently, the spatial extent of interictal-like activity represents the mean percentage of MEA channels that recorded extracellular signals for all ILEs belonging to the major cluster. On average, we observed that interictal-like activity in *Dcx*-KD and mismatch rats spread over similarly extended neocortical areas, although a nonsignificantly smaller spatial extent appeared to be involved in *Dcx*-KD rats ($67.6 \pm 7.4\%$ MEA channels in mismatch rats and $51.9 \pm 5.7\%$ in *Dcx*-KD rats; unpaired *t* test, $p = 0.1$; Fig 4). On the pixel maps we constructed for representing the spatial extent of interictal-like activity, we noticed that neocortical areas covered by MEA channels that recorded the most important number of ILEs always included SBH (dark area in Fig 4A), suggesting that a large proportion of these events propagate to SBH. We then measured in *Dcx*-KD rats the propagation delays between an MEA channel located at the spatial origin of onset in the normotopic cortex, and an MEA channel located in SBH. We found that ILEs originating in the normotopic cortex in *Dcx*-KD rats propagated to SBH in 31.35 ± 8.76 milliseconds, where MUA was simultaneously detected. In parallel, we measured in both mismatch and *Dcx*-KD rats the propagation delays between an MEA channel located at the origin, and an MEA channel located in deep neocortical layers close to the anatomical reference. On average, ILEs originating in the normotopic cortex propagated to deep cortical layers with similar delays in *Dcx*-KD and mismatch rats (49.01 ± 18.11 milliseconds in *Dcx*-KD rats and 59.17 ± 20.90 milliseconds in mismatch; Mann–Whitney test, $p = 0.7$), both being associated with similar levels of MUA ($38.24 \pm 12.37\%$ of ILEs in *Dcx*-KD and $32.94 \pm 11.59\%$ in mismatch). Importantly, we observed that the great majority of ILEs ($97.6 \pm 2.4\%$) originating in the normotopic cortex secondarily propagated to SBH, suggesting that SBH was intricately integrated within the cortical network and participated to interictal-like activity together with the normotopic cortex. To further study this issue for individual ILEs, we plotted as a function of time the recruitment onsets of all MEA channels and identified among SBH-located channels which

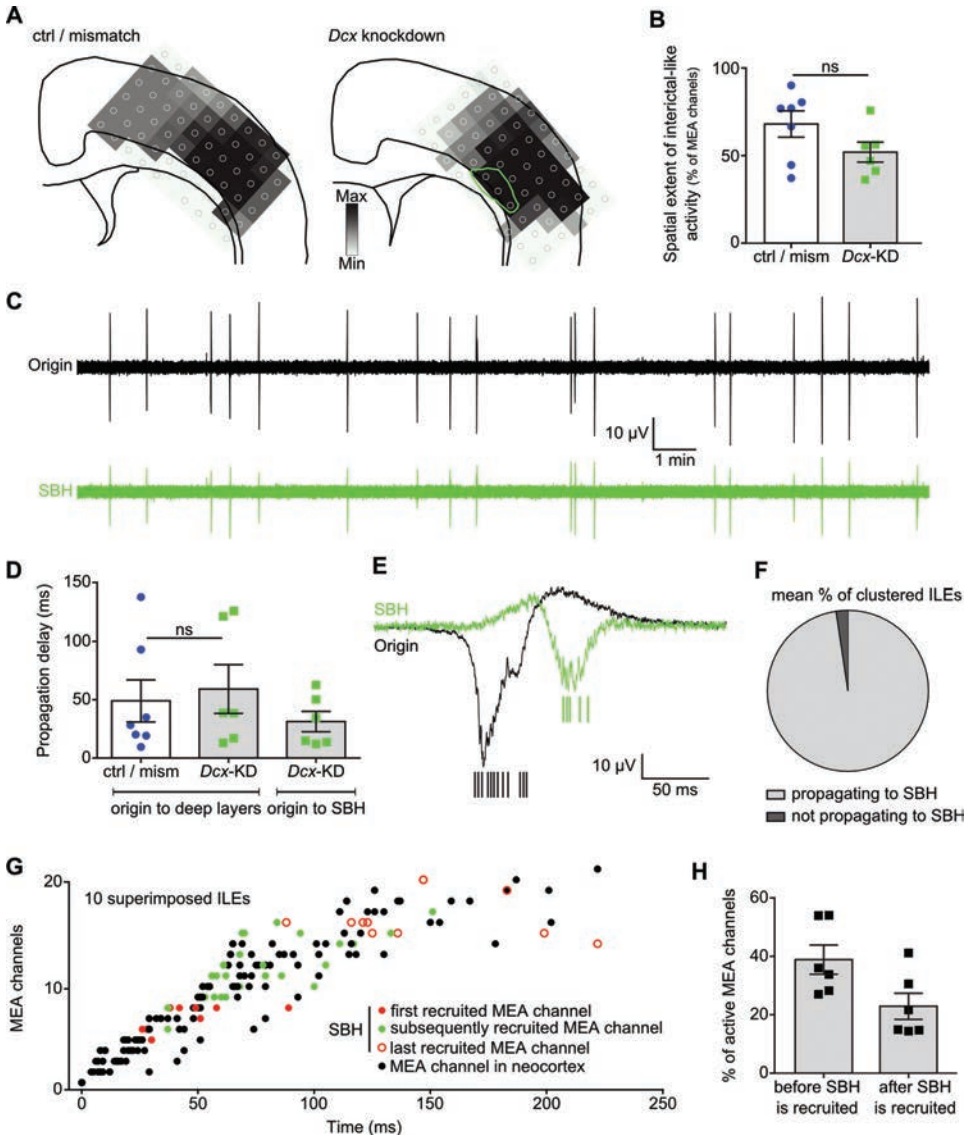

FIGURE 4: Interictal-like activity originating in the overlying cortex secondarily propagates to subcortical band heterotopia (SBH). (A) Representative pixel maps showing the minimal (gray) and maximal (black) neocortical area exhibiting interictal-like activity in a control (ctrl)/mismatch (left) and in a *Dcx*-KD (right) rat. SBH boundaries are delineated in green. (B) Bar graphs and scatter dot plots illustrating the spatial extent of interictal-like activity in control/mismatch (mism) and *Dcx*-KD rats. MEA = microelectrode array; ns = not significant. (C) Interictal-like activity in a *Dcx*-KD rat, as simultaneously recorded from 2 MEA channels located at the spatial origin of onset in the normotopic cortex *(black trace)* and in SBH *(green trace)*. (D) Bar graphs and scatter dot plots illustrating interictal-like event propagation delays between an MEA channel located at the spatial origin of onset and an MEA channel located in deep neocortical layers or in SBH in control/mismatch and *Dcx*-KD rats. (E) A Representative interictal-like event, as simultaneously recorded from 2 MEA channels located at the spatial origin of onset in the normotopic cortex *(black trace)* and in SBH *(green trace)*. Multiple units are represented by vertical bars under local field potential events. (F) Pie chart illustrating the mean percentage of interictal-like events (ILEs) originating in the normotopic cortex that propagate to SBH in *Dcx*-KD rats. (G) Raster plot of MEA channel recruitment onsets as a function of time for 10 superimposed ILEs in a *Dcx*-KD rat. (H) Bar graphs and scatter dot plots showing the mean percentage of MEA channels active before/after SBH-located MEA channels are recruited. Interictal-like activity from n = 7 control/mismatch rats and n = 6 *Dcx*-KD rats was analyzed. Mean values ± standard error of mean are given.

channel was recruited first, which channels were recruited next, and which channel was recruited last. A visual inspection of the recruitment dynamics for several superimposed ILEs revealed that SBH-located channels could be recruited at nearly any time during the course of an event, with the exception of the early phase of this event and, to a lesser extent, its late phase. We then quantified the mean percentage of MEA channels that were active before the first MEA channel located in SBH is recruited, and found that 38.8 ± 4.9% of channels were active. After the last SBH-located MEA channel is recruited, 22.9 ± 4.4% of channels were found active.

Together, these observations show that interictal-like activity in *Dcx*-KD rats originating in the overlying cortex secondarily propagates to SBH.

In Vivo Suppression of Neuronal Excitability in the Normotopic Cortex but Not in SBH Mitigates Seizure Susceptibility in Dcx-KD Rats

Our observations made on neocortical slices suggested a major role of the normotopic cortex over the band heterotopia for generating interictal-like epileptiform activity. We thus reasoned that manipulating neuronal excitability within the normotopic cortex could influence the propensity for induced seizures in *Dcx*-KD rats in vivo, whereas the same manipulation in SBH would be less effective. To test this hypothesis, we created rats with SBH expressing either in SBH alone, or in SBH and in the normotopic cortex, an inwardly rectifying potassium channel, Kir2.1, previously utilized for chronically suppressing neuronal excitability.[25,26] Neurons expressing Kir2.1 were confirmed to display a significantly more hyperpolarized resting membrane potential than controls on cultivated and acute slices, consistent with a decreased neuronal excitability (cultivated slices: -40.9 ± 3.5mV in controls and -63.4 ± 3.6mV in Kir2.1-expressing neurons, Mann–Whitney test, $p < 0.001$, 10 neurons per condition; acute slices: -68.9 ± 2.2mV in controls and -77.6 ± 1.1mV in Kir2.1-expressing neurons, unpaired t test, $p < 0.05$, 6 and 5 neurons per condition).

Dcx-KD rats with silenced SBH were created using in utero electroporation, by injection and coelectroporation of RFP and Kir2.1 expression plasmids together with plasmids encoding shRNAs against *Dcx* 3′UTR. Patch clamp recordings confirmed that 90 to 100% of fluorescent neurons coelectroporated with Kir2.1 plasmids functionally expressed Kir2.1 channels, suggesting that SBH composed of Kir2.1-expressing neurons displayed decreased excitability. Accordingly, extracellular recordings on slices from animals with Kir2.1-expressing SBH revealed that a reduced proportion of events propagated to SBH ($34.4 \pm 10.5\%$ of events, 3 slices), as compared to animals with normally active SBH ($97.6 \pm 2.4\%$ of events, see Fig 4F). In addition, events propagating to SBH had very low amplitude (6.3 ± 0.7 μV in SBH and 164.7 ± 42.1 μV at the origin of onset in the normotopic cortex). Together, these observations suggest that SBH composed of Kir2.1-expressing neurons are less likely to be engaged in network-driven epileptiform activity.

We created *Dcx*-KD rats with silenced SBH and normotopic cortex using in utero electroporation and a 2-step procedure. We first injected and electroporated Kir2.1 and GFP expression plasmids to transfect neurons in the normotopic cortex; then, 30 minutes later, we injected and electroporated RFP expression plasmids together with plasmids encoding shRNAs against *Dcx* 3′UTR to initiate SBH formation. In all *Dcx*-KD rats with silenced SBH and normotopic cortex (14 rats), transfected neurons expressing GFP were found in the normotopic cortex, and in 7 of 14 rats the transfected area included the portion of neocortex directly facing SBH (Fig 5A). In SBH, $71.67 \pm 18.45\%$ of RFP-transfected neurons were found to coexpress GFP (see Fig 5B). Given that 90 to 100% of fluorescent neurons coelectroporated with Kir2.1 plasmids functionally expressed Kir2.1 channels, these data suggest that large numbers of neurons located in the normotopic cortex and, to a lesser extent, in SBH were efficiently silenced in *Dcx*-KD rats generated using this procedure. Accordingly, extracellular recordings on slices from animals expressing Kir2.1 channels in the normotopic cortex and SBH revealed that lower numbers of epileptiform events could be recorded from the Kir2.1-expressing normotopic cortex ($27.9 \pm 7.8\%$ of ILEs, 3 rats), as compared to those recorded from the normotopic cortex of *Dcx*-KD rats with normally active SBH ($72.2 \pm 9.7\%$ of ILEs, 5 rats). These observations suggest that portions of neocortex composed of Kir2.1-expressing neurons are less likely to be engaged in network-driven epileptiform activity.

Three groups of *Dcx*-KD rats were then analyzed for their susceptibility to PTZ-induced seizures using intracortical EEG recordings: *Dcx*-KD rats with normally active SBH (10 rats), *Dcx*-KD with silenced SBH (10 rats), and *Dcx*-KD rats with silenced SBH and normotopic cortex (14 rats). Whereas *Dcx*-KD rats with silenced SBH displayed electrographic seizures at similar doses and latencies as compared to *Dcx*-KD rats with normally active SBH, we found that *Dcx*-KD rats with silenced SBH and normotopic cortex exhibited significantly longer latencies to seizure ($1{,}755 \pm 78.99$ seconds in *Dcx*-KD rats with normally active SBH; $1{,}506 \pm 68.54$ seconds in *Dcx*-KD rats with silenced SBH; $2{,}086 \pm 267.40$ seconds in *Dcx*-KD rats with silenced SBH and normotopic cortex; log-rank test, $p < 0.05$; see Fig 5C, D). Moreover, the proportion of *Dcx*-KD rats exhibiting seizures with >3 PTZ injections was significantly higher in *Dcx*-KD rats with silenced SBH and normotopic cortex, as compared to *Dcx*-KD rats with normally active SBH and *Dcx*-KD rats with silenced SBH (57% of *Dcx*-KD rats with silenced normotopic cortex and SBH, 30% of *Dcx*-KD rats with normally active SBH, 20% of *Dcx*-KD rats with silenced SBH; chi-square test, $p < 0.01$; see Fig 5E).

These results show that a chronic suppression of neuronal excitability in SBH alone does not modify the

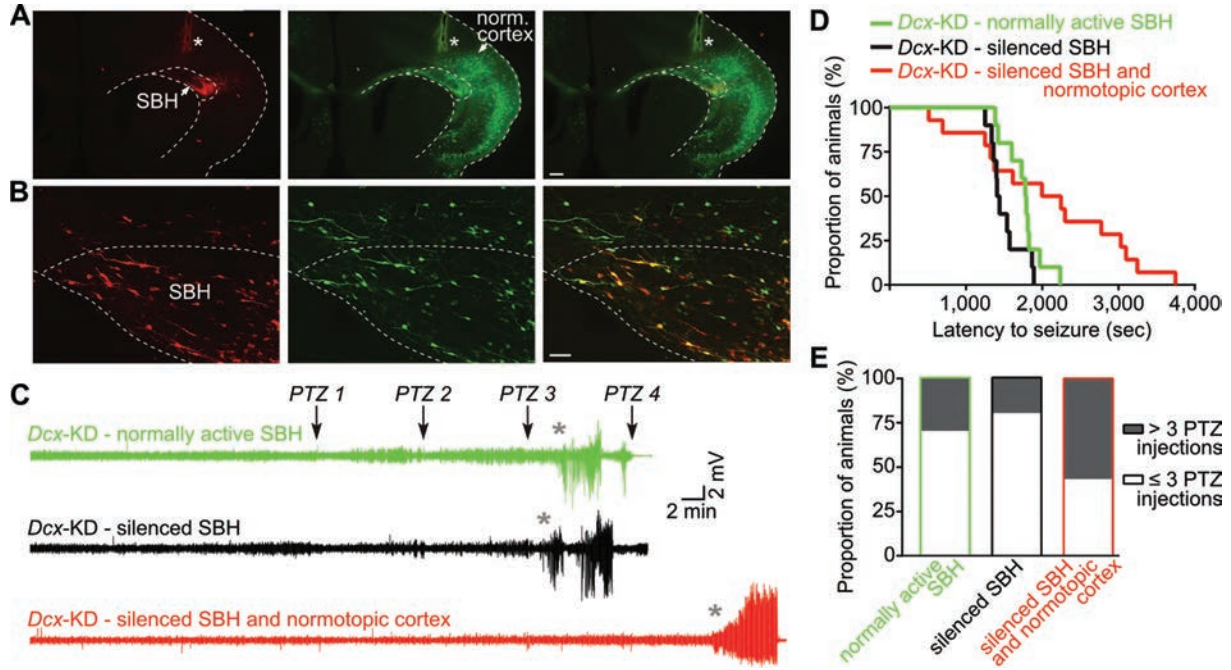

FIGURE 5: In vivo suppression of neuronal excitability in the normotopic cortex but not in subcortical band heterotopia (SBH) mitigates seizure susceptibility in *Dcx*-KD rats. (A) Low-magnification fluorescent microphotographs of a neocortical section from a *Dcx*-KD rat with silenced SBH and normotopic (norm.) cortex, as obtained after the 2-step in utero electroporation procedure. The left panel shows the red fluorescent protein (RFP)-expressing population (in red) forming SBH, and the middle panel shows the green fluorescent protein (GFP)-expressing population (in green) located in the normotopic cortex. Red and green channels are merged in the right panel. Asterisks indicate the tract of the recording electrode within the primary somatosensory cortex. Scale bar = 500μm. (B) High-magnification confocal microphotographs of the same section as in A, taken at the level of the medial end of SBH. The left panel shows RFP-expressing neurons (in red) cotransfected with plasmids encoding shRNAs against *Dcx*, and the middle panel shows GFP-expressing neurons (in green) cotransfected with plasmids expressing Kir2.1 channels. In the right panel, where red and green channels are merged, note the high proportion of neurons (in yellow) coexpressing the 2 reporter genes *GFP* and *RFP*. Z-projection of 48 planes (Z-step = 0.5μm); scale bar = 50μm. (C) Three representative intracortical electroencephalograms showing pentylenetetrazol (PTZ)-induced seizures, as recorded in the right hemispheres of a *Dcx*-KD rat with normally active SBH *(green trace)*, a *Dcx*-KD rat with silenced SBH *(black trace)*, and a *Dcx*-KD rat with silenced SBH and normotopic cortex *(red trace)*. PTZ was administered every 10 minutes until a seizure occurred (*asterisks* indicate seizure onsets), and diazepam was given to stop seizures lasting >5 minutes. (D) Survival curve showing the latency to PTZ-induced seizure in the 3 groups of *Dcx*-KD rats. Seizures in *Dcx*-KD rats with silenced SBH and normotopic cortex occurred with a significantly longer latency when compared with *Dcx*-KD with normally active SBH and with *Dcx*-KD rats with silenced SBH (log-rank test, $p < 0.01$). (E) Bar graph illustrating the proportion of animals expressing seizures triggered with less or more than 3 PTZ injections. A significantly higher proportion of animals in *Dcx*-KD rats with silenced SBH and normotopic cortex exhibited seizures with >3 PTZ injections, as compared to other groups (chi-square test, $p < 0.01$). Ten *Dcx*-KD rats with normally active SBH, 10 *Dcx*-KD rats with silenced SBH, and 14 *Dcx*-KD rats with silenced SBH and normotopic cortex were analyzed.

higher propensity of *Dcx*-KD rats to display seizures, whereas the same manipulation within the normotopic cortex and SBH ameliorates seizure susceptibility. Together, these data suggest that the normotopic cortex on its own may contribute to seizure susceptibility in *Dcx*-KD rats.

Discussion

Consequences of altered cortical development include neurodevelopmental delay and, in most cases, drug-resistant seizures. In patients with SBH, conducted studies were unable to clarify which of the 2 structures is the most critical for generating epileptiform activities, although all suggested that both the heterotopic band and normotopic cortex contribute to epileptic manifestations. In the present study conducted in a targeted genetic model of SBH in rats, we show that (1) the presence of a band heterotopia resembling SBH seen in patients is associated in rats with an altered neocortical circuitry prone to generate epileptiform activity; (2) although participating to interictal-like activity together with the normotopic cortex, the band heterotopia does not constitute a primary origin for epileptiform discharges in vitro and is dispensable for generating seizures in vivo; and (3) the normotopic cortex overlying SBH originates interictal-like activity in vitro, and a chronic suppression of its excitability mitigates seizure susceptibility levels in vivo, confirming its major role over the band heterotopia for generating epileptiform activity.

Depth recordings in SBH are rarely available, because patients are not good candidates for epilepsy surgery given its poor outcome in the few reported cases.[12] However, from the reported cases, epileptiform discharges starting outside SBH and secondarily propagating to both the heterotopic and normotopic cortices were described in 1 patient,[27] and a patient with no epileptiform activity recorded from SBH was also reported.[12] Together with the observations made from our animal model, these electroclinical studies support the notion that the normally migrated cortex surrounding the band heterotopia may play a major role in generating epileptiform discharges in patients as well.

Other pathological conditions in which the dysplastic or lesioned brain area is not the primary origin of epileptiform activity have been described. In tuberous sclerosis complex (TSC), electrocorticographic (ECoG) recordings with depth electrodes and subdural grids placed within tubers and perituberal cortex have revealed epileptiform activity and ictal onsets in the perituberal cortex in a few patients, whereas the tuber remained electrographically silent in some cases.[28–30] Although surgical removal of tubers has been found effective to achieve seizure freedom in several TSC cases,[31] patients with ECoG-recorded epileptiform discharges that remained even after the presumably epileptogenic tuber was surgically removed were also described.[32] Together, these observations in TSC patients suggest that epileptiform activity may derive from the normal-appearing cortex surrounding a dysplastic area.

Similarly, epileptiform activity associated with focal lesions such as brain tumors or cavernous angiomas was suggested to originate in the adjacent cortex. Noninvasive assessment of focal epileptic activity using magnetoencephalography (MEG) in patients with a single cavernous angioma revealed MEG spikes at the lesion border,[33] and spontaneous bursting activity was recorded from neurons adjacent to cavernomas in resected tissue.[34] In patients with brain tumors, epileptiform activity was predominantly recorded overlying the tumor, the tumor core usually being electrographically silent, although "spiking tumor cells" were described in some cases. Studies in patients with glioma revealed epileptiform activity at the tumor border, not within the core,[35] and spontaneous epileptiform activity was recorded in glioma-transplanted mice both in vivo and on acute slices,[36] originating at a distance from the tumor.[37] Again, these observations suggest that the adjacent cortex may be more epileptogenic than the lesion itself.

Mechanisms underlying epileptogenicity in brains with SBH are still unclear, but observations obtained from experimental SBH suggested that these mechanisms likely combine interdependent circuit-level defects and abnormal intrinsic features of both misplaced and normally positioned neurons. In *Dcx*-KD rats, neurons in SBH were found to display a delayed maturation of GABAergic synapses, whereas neurons in the normally migrated cortex exhibited a massive increase of ongoing glutamatergic synaptic currents. In addition, SBH neurons were found to send axonal collaterals to deep layers of the normally migrated cortex, as well as long run axons reaching the contralateral cortex, striatum, or thalamus. Such abnormal features were never observed in the neocortex of mismatch or nonelectroporated controls.[14] If the band heterotopia in *Dcx*-KD rats did not seem to originate epileptiform activity, this activity however generally propagated to it, as we studied here in vitro. In this context, axonal projections from SBH may provide a morphological substrate for distributing epileptiform activity to distant, abnormally connected brain areas, similarly to what was described in an animal model of periventricular nodular heterotopia.[38–40] Collectively, these observations in *Dcx*-KD rats may help draw a plausible scenario combining increased neuronal excitability and abnormal circuitry, both contributing to favor the emergence of seizures from the normally migrated cortex. Whether other brain areas located upstream or downstream from this epileptogenic network could also contribute to epileptiform activity, as suggested in human patients will focal lesions,[41] remains an open question. Last, although rodent models of epileptogenic cortical malformations offer valuable insight into the causes and mechanisms of difficult to treat epilepsies, one could reasonably assume that certain cellular mechanisms, seizure propagation pathways, or clinical manifestations are more complex in humans and inaccessible to investigation in rodents.

Although not the primary purpose of the present study, the ameliorated seizure phenotype we obtained by chronically suppressing excitability with overexpressed Kir2.1 channels may help in envisioning novel therapeutic strategies. Experimental studies reporting ameliorated epilepsy phenotype after modifying excitability using brain-delivered viruses expressing potassium channels were recently published. In a rat model of refractory neocortical epilepsy obtained by microinjecting tetanus toxin in the rat motor cortex, concomitant injection of Kv1.1-expressing lentiviruses was found to significantly decrease the number of epileptiform events.[42] An engineered TREK-1 channel with enhanced constitutive activity and insensitivity to intracellular regulation mechanisms was also found to be efficient in reducing spontaneous firing of cultured neurons expressing a mutated Cav3.2 channel found in patients with absence epilepsy. Moreover,

adenovirus-mediated expression of this engineered TREK-1 channel was associated with a decreased duration of status epilepticus in the lithium-pilocarpine model.[43] We could speculate that similar strategies utilizing conditionally expressed or externally delivered Kir2.1 or other types of potassium channels in the neocortex may also ameliorate the phenotype in *Dcx*-KD rats, including in adults with spontaneous seizures.[16]

Acknowledgment

The is study was supported by the French National Agency for Research (RPDOC#RPV09010AAA, J.-B.M.; Samenta #19012012, A.R.), Fondation Jérôme Lejeune (R12013AAAA, J.-B.M.), Région Provence Alpes Côte d'Azur (APEX2012, J.-B.M.), Fédération pour la Recherche sur le Cerveau/Rotary (Espoir en tête 2009, A.R.), European Community 7th Framework program THEME (HEALTH.2013.2.2.1-4, A.R.), and Ligue Française Contre l'Epilepsie (M.J.).

We thank Dr J. LoTurco for *Dcx* shRNAs plasmids and helpful discussions; Dr Y. Tagawa for Kir2.1 plasmids; Drs R. Khazipov and M. Minlebeav for their help with in vivo recordings; Drs L. Anikstejn, R. Cossart, V. Crepel, and M. Milh for helpful discussions; Dr H. Becq for in utero electroporations in the early stage of the project; and F. Bader for animal care.

Authorship

L.F.P. performed MEA recordings and developed analysis tools; M.J. performed in vivo recordings and histological analyses; E.B. generated *Dcx*-KD rats; A.M. developed analysis tools; A.P. performed slice culture and patch clamp recordings; Y.C. performed histological analyses; F.W. performed cell culture experiments and molecular biology; L.F.P., M.J., A.P., Y.C., F.W., and J.-B.M. analyzed the data; J.-B.M., A.R., L.F.P., and M.J. designed the study and wrote the paper. L.F.P. and M.J. contributed equally.

Potential Conflicts of Interest

Nothing to report.

References

1. Barkovich AJ, Jackson DE Jr, Boyer RS. Radiology. 1989;171:455–458.
2. Gleeson JG, Allen KM, Fox JW, et al. Doublecortin, a brain-specific gene mutated in human X-linked lissencephaly and double cortex syndrome, encodes a putative signaling protein. Cell 1998;92:63–72.
3. Pilz DT, Matsumoto N, Minnerath S, et al. LIS1 and XLIS (DCX) mutations cause most classical lissencephaly, but different patterns of malformation. Hum Mol Genet 1998;7:2029–2037.
4. Pinard JM, Motte J, Chiron C, et al. Subcortical laminar heterotopia and lissencephaly in two families: a single X linked dominant gene. J Neurol Neurosurg Psychiatry 1994;57:914–920.
5. des Portes V, Francis F, Pinard JM, et al. Doublecortin is the major gene causing X-linked subcortical laminar heterotopia (SCLH). Hum Mol Genet 1998;7:1063–1070.
6. D'Agostino MD, Bernasconi A, Das S, et al. Subcortical band heterotopia (SBH) in males: clinical, imaging and genetic findings in comparison with females. Brain 2002;125:2507–2522.
7. Guerrini R, Sicca F, Parmeggiani L. Epilepsy and malformations of the cerebral cortex. Epileptic Disord 2003;5(suppl 2):S9–S26.
8. Bahi-Buisson N, Souville I, Fourniol FJ, et al. New insights into genotype-phenotype correlations for the doublecortin-related lissencephaly spectrum. Brain 2013;136:223–244.
9. Matsumoto N, Leventer RJ, Kuc JA, et al. Mutation analysis of the DCX gene and genotype/phenotype correlation in subcortical band heterotopia. Eur J Hum Genet 2001;9:5–12.
10. Dobyns WB. The clinical patterns and molecular genetics of lissencephaly and subcortical band heterotopia. Epilepsia 2010; 51(suppl 1):5–9.
11. Tanaka T, Gleeson JG. Subcortical laminar (band) heterotopia. Handb Clin Neurol 2007;87:191–204.
12. Bernasconi A, Martinez V, Rosa-Neto P, et al. Surgical resection for intractable epilepsy in double cortex syndrome yields inadequate results. Epilepsia 2001;42:1124–1129.
13. Mai R, Tassi L, Cossu M, et al. A neuropathological, stereo-EEG, and MRI study of subcortical band heterotopia. Neurology 2003; 60:1834–1838.
14. Ackman JB, Anikstejn L, Crépel V, et al. Abnormal network activity in a targeted genetic model of human double cortex. J Neurosci 2009;29:313–327.
15. Bai J, Ramos RL, Ackman JB, et al. RNAi reveals doublecortin is required for radial migration in rat neocortex. Nat Neurosci 2003; 6:1277–1283.
16. Lapray D, Popova I, Kindler J, et al. Spontaneous epileptic manifestations in a DCX knockdown model of human double cortex. Cereb Cortex 2010;20:2694–2701.
17. Manent J, Wang Y, Chang Y, et al. Dcx reexpression reduces subcortical band heterotopia and seizure threshold in an animal model of neuronal migration disorder. Nat Med 2009;15:84–90.
18. Ramos RL, Bai J, LoTurco JJ. Heterotopia formation in rat but not mouse neocortex after RNA interference knockdown of DCX. Cereb Cortex 2006;16:1323–1331.
19. Matsuda T, Cepko CL. Controlled expression of transgenes introduced by in vivo electroporation. Proc Natl Acad Sci U S A 2007; 104:1027–1032.
20. Khazipov R, Sirota A, Leinekugel X, et al. Early motor activity drives spindle bursts in the developing somatosensory cortex. Nature 2004;432:758–761.
21. Schindelin J, Arganda-Carreras I, Frise E, et al. Fiji: an open-source platform for biological-image analysis. Nat Methods 2012;9:676–682.
22. Steidl E, Neveu E, Bertrand D, Buisson B. The adult rat hippocampal slice revisited with multi-electrode arrays. Brain Res 2006; 1096:70–84.
23. Feldt Muldoon S, Soltesz I, Cossart R. Spatially clustered neuronal assemblies comprise the microstructure of synchrony in chronically epileptic networks. Proc Natl Acad Sci U S A 2013;110:3567–3572.
24. Nicholson C, Freeman JA. Theory of current source-density analysis and determination of conductivity tensor for anuran cerebellum. J Neurophysiol 1975;38:356–368.
25. Burrone J, O'Byrne M, Murthy VN. Multiple forms of synaptic plasticity triggered by selective suppression of activity in individual neurons. Nature 2002;420:414–418.

26. Mizuno H, Hirano T, Tagawa Y. Evidence for activity-dependent cortical wiring: formation of interhemispheric connections in neonatal mouse visual cortex requires projection neuron activity. J Neurosci 2007;27:6760–6770.
27. Lo Russo G, Tassi L, Cossu M, et al. Focal cortical resection in malformations of cortical development. Epileptic Disord 2003; 5(suppl 2):S115–S123.
28. Ma TS, Elliott RE, Ruppe V, et al. Electrocorticographic evidence of perituberal cortex epileptogenicity in tuberous sclerosis complex. J Neurosurg Pediatr 2012;10:376–382.
29. Madhavan D, Weiner HL, Carlson C, et al. Local epileptogenic networks in tuberous sclerosis complex: a case review. Epilepsy Behav 2007;11:140–146.
30. Major P, Rakowski S, Simon MV, et al. Are cortical tubers epileptogenic? Evidence from electrocorticography. Epilepsia 2009;50: 147–154.
31. Koh S, Jayakar P, Dunoyer C, et al. Epilepsy surgery in children with tuberous sclerosis complex: presurgical evaluation and outcome. Epilepsia 2000;41:1206–1213.
32. Chandra PS, Salamon N, Huang J, et al. FDG-PET/MRI coregistration and diffusion-tensor imaging distinguish epileptogenic tubers and cortex in patients with tuberous sclerosis complex: a preliminary report. Epilepsia 2006;47:1543–1549.
33. Stefan H, Scheler G, Hummel C, et al. Magnetoencephalography (MEG) predicts focal epileptogenicity in cavernomas. J Neurol Neurosurg Psychiatry 2004;75:1309–1313.
34. Williamson A, Patrylo PR, Lee S, Spencer DD. Physiology of human cortical neurons adjacent to cavernous malformations and tumors. Epilepsia 2003;44:1413–1419.
35. Patt S, Steenbeck J, Hochstetter A, et al. Source localization and possible causes of interictal epileptic activity in tumor-associated epilepsy. Neurobiol Dis 2000;7:260–269.
36. Buckingham SC, Campbell SL, Haas BR, et al. Glutamate release by primary brain tumors induces epileptic activity. Nat Med 2011; 17:1269–1274.
37. Kohling R, Senner V, Paulus W, Speckmann E. Epileptiform activity preferentially arises outside tumor invasion zone in glioma xenotransplants. Neurobiol Dis 2006;22:64–75.
38. Chevassus-Au-Louis N, Congar P, Represa A, et al. Neuronal migration disorders: heterotopic neocortical neurons in CA1 provide a bridge between the hippocampus and the neocortex. Proc Natl Acad Sci U S A 1998;95:10263–10268.
39. Chevassus-Au-Louis N, Jorquera I, Ben-Ari Y, Represa A. Abnormal connections in the malformed cortex of rats with prenatal treatment with methylazoxymethanol may support hyperexcitability. Dev Neurosci 1999;21:385–392.
40. Tschuluun N, Jurgen Wenzel H, Doisy ET, Schwartzkroin PA. Initiation of epileptiform activity in a rat model of periventricular nodular heterotopia. Epilepsia 2011;52:2304–2314.
41. Aubert S, Wendling F, Regis J, et al. Local and remote epileptogenicity in focal cortical dysplasias and neurodevelopmental tumours. Brain 2009;132:3072–3086.
42. Wykes RC, Heeroma JH, Mantoan L, et al. Optogenetic and potassium channel gene therapy in a rodent model of focal neocortical epilepsy. Sci Transl Med 2012;4:161ra152.
43. Dey D, Eckle V, Vitko I, et al. A potassium leak channel silences hyperactive neurons and ameliorates status epilepticus. Epilepsia 2014;55:203–213.